SSRG International Journal of Mechanical Engineering
ISSN: 2348-8360/ https://doi.org/10.14445/23488360/IJME-V11I9P104

Volume 11 Issue 9, 53-64, September 2024

Original Article

Parametric Optimization and Microhardness Analysis in DED Single-layer Stellite-6

Sunil V. Patel[1], Chirag P. Patel[2]

[1]*Faculty of Engineering and Technology, Ganpat University, Mehsana, Gujarat, India.*
[2]*Department of Mechanical Engineering, FoET, Ganpat University, Mehsana, Gujarat, India.*

[1]*Corresponding Author : sunil1.patel@ganpatuniversity.ac.in*

Received: 10 July 2024 Revised: 13 August 2024 Accepted: 12 September 2024 Published: 30 September 2024

Abstract *- The utilization of Direct Energy Deposition (DED) through the laser cladding process presents a significant opportunity for enhancing the production of high-performance steel. This research delves into the parametric performance and micro-hardness assessment of a Stellite-6 layer deposited onto SS316 substrates via laser coating. Stellite-6 is renowned for its exceptional wear and corrosion resistance, rendering it a favorable option for enhancing the surface of the widely utilized SS316. Studies define the impact of various parameters (such as laser power, laser scan speed, powder quantity, etc.) on the microstructure and micro-hardness characteristics of SS316 and Stellite-6. Micro-hardness evaluations were conducted to ascertain the coating's hardness distribution and area. The interface between the substrate and the coating was also examined. Furthermore, the influence of permeability on coating height and depth was investigated. These findings offer insights into the process quality necessary to attain the desired strength and enhance comprehension of the micro-structural attributes of laser-coated Stellite-6 on SS316 substrate systems.*

Keywords *- Direct energy deposition, Micro-hardness analysis, Laser cladding, Stellite-6, SS316.*

1. Introduction - LCP

Since the inception of the first operational laser by Theodore Maiman in 1960, the laser industry has experienced an annual growth rate of approximately 10-20%. These developments are driven by increasing laser applications, which represent a form of optical energy. In the past decades, laser exertion has been found in a wide range of sectors, including mensuration, snapping, physical refinement, therapy, electronics and communications. In the prefabricate domain, the beam intensity is transformed into warm intensity by concentrating the ray beam onto a designated spot size profile through an optical arrangement. During interaction between the laser and processing materials generates structural vibrations that produce heat that is sufficient to melt the material by converting optical energy into thermal energy. Owing to its versatility and ease of automation, laser technology is highly adaptable for numerous applications. In manufacturing, lasers were utilized in various applications such as fusing, rehearsing, cladding, buffing, surface flushing, surface behavior, micro-machining, buckling, additive manufacturing 3D marking and cutting [3, 5, 6]. Lasers are produced by energizing gaining medium, whether it is from frozen, liquor or vapor, using an intensity origin such as a flash of glow, electric current or thermal from other sources. This energization prompts the electrons to shift from a low-vitality state to a high-vitality state within the same medium. As these electrons come back to their lower energy state, they emit quantum, which is in the shape of glow vitality. These photons engage with the way situated in the middle of two reflectors-one totally reflective and the other to some extent reflective, while seen in CO_2 lasers, or between two Bragg gratings, as in fiber lasers. This interaction amplifies the number of photons, and as their population increases, a specific wavelength is attained, resulting in an orderly, achromatic beam. This beam subsequently runs through, to some extent, a reflective reflector or display and is directed by optic components such as collimating and focusing lenses for various manufacturing applications [8]. The Direct Energy Deposition (DED) techniques, including laser cladding, have emerged as versatile additive manufacturing processes for fabricating complex metal parts with enhanced properties.

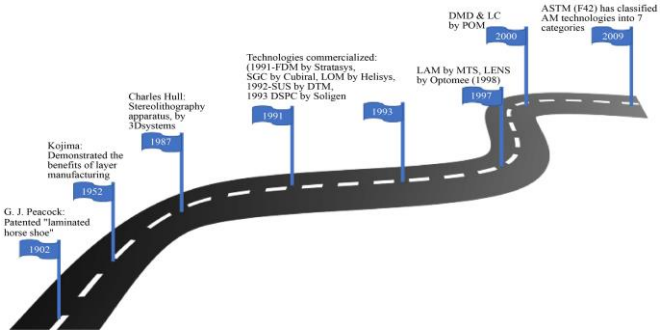

Fig. 1 History of Additive Manufacturing (AM)

The process of applying material to a base using a huge-energy ray beam is known as laser cladding, enabling precise control over the deposited material and the ability to tailor properties to meet specific application requirements. Stellite-6, a cobalt-based alloy, is well-known for its exceptional scratch and imperviable, making it an attractive alternative for various high-performance supplication. In this study, we investigate the parametric optimization and micro-hardness analysis of single-layer Stellite-6 deposited on SS316 substrate using the LCP. SS316 is a broadly pre-owned stainless steel alloy valued for its corrosion resistance and mechanical properties.

2. Literature Review

Work on the evolution of operational classified pieces can be promoted and undergo more mechanical testing to inaugurate the integrity of classified pieces produced [9]. LC parts can reach most provisions for wear and corrosion resistance.

Table 1. Literature review [12]

Features	Surface Deposition Processes			
	Laser Cladding	**Thermal Spray**	**Chemical Vapour Deposition**	**Physical Vapour Deposition**
Bonding Strength	High	Moderate	Low	Low
Dilution	High	Nil	Nil	Nil
Coating Material	Metals, Ceramics	Metals, Ceramics	Metals, Ceramics	Metals, Ceramics
Coating Thickness	50µm to Not Limited	50µm to Several Limited	0.05 µm to 20 µm	0.05 µm to 10 µm
Repeatability	Moderate to High	Moderate	High	High
Heat Affected Zone	Low	High	Very Low	Very Low
Controllability	Moderate to High	Moderate	Moderate to High	Moderate to High
Cost	High	Moderate	High	High

Although, some appeal-oriented challenges like severe wear, peculiar erosion-corrosion, debility, excessive thermal worm, and severe erosion are necessary for the exploration of lucrative appeal [10]. These work from experimental research to Industrial Applications [11]. A work on collation between LC and other covering techniques [12]. LC, a cutting-edge technique widely employed across various industries, serves the purpose of fortifying substrates against oxidation, corrosion, and wear [13-20]. This method involves depositing a protective layer, known as a "siding substance," onto a base metal using thermal vitality from a laser beam. Typically, the siding substance is applied to the substrate either through wire feed or powder feed, with the latter being more common due to its greater flexibility [21-23]. The versatility of laser cladding extends its application to sectors such as mining, metallurgy, aerospace, automotive, marine, and biomedical industries [24-26]. Unlike conventional surface modification methods, laser cladding offers finer grain size, enhanced fusible copulation with the substrate, reduced dilution, and fewer warm-infected zones [27-34].

However, achieving optimal coating quality relies heavily on controlling the cladding process parameters efficiently. Laser cladding boasts advantages such as minimal substrate heat effect, high precision, and superior quality [35-39]. Moreover, recent advancements in laser cladding research explore the integration of ultrasonic vibration to further enhance coating quality. Drawing inspiration from ultrasonography in welding, this innovative approach aims to refine grain structures, homogenize microstructures, and alleviate residual stress, ultimately improving the bonding between coatings and substrates [40, 41].

3. Summary of Literature Review and Problem Identification

From the literature, it is clear that a few works have been carried out in the recent past on laser cladding using Mo (Molybdenum) and W (Tungsten) as potential materials for corrosion resistance and wear resistance coating. Upon going through the literature, it is concluded that laser cladding produces better surface coating compared to any other surface coating techniques. Further, Stellite-6 was used for coating the base material SS316. Hence, stellite-6 is identified as a potential coating material. Having identified the importance of SS316 material in the mechanical industries and 3D printing technology developments in recent days, it is decided to carry out the present research by coating stellite-6 on SS316 substrate material by employing laser cladding techniques.

4. Materials and Methods

SS316 was selected as the base material to examine the depth of stellite-6 coating powder on the substrate. 25 × 20 × 8 mm^3 SS316 cuboid was chosen because it fits the existing large structure. For the experiment, aerosolized stellite-6 powder was purchased from Indo-Mim Pvt. provided by. Ltd. India was doing this.

Analysis using JEOL 6380A tungsten W-SEM publicized that Stellite-6 metal powder tiny bits are mostly globe-shaped with dimensions from 60 to 140 µm, as revealed in Figure 2. Synthetic substance analysis of SS316 and coating powder was performed using XRF analysis and EDX-7000 equipment. The results are given in Tables 2 and 3, respectively, laser energy.

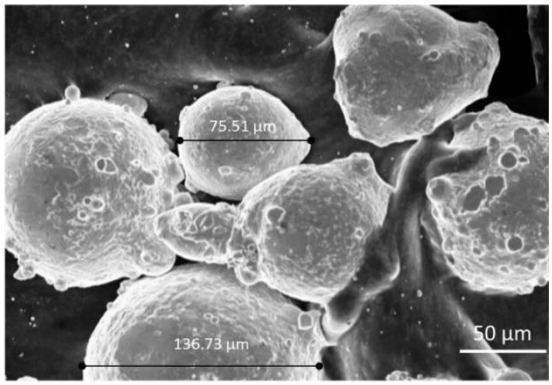

Fig. 2 SEM morphology of stellite-6 alloy powder

Research began with the first single-layer coating test using Stellite-6, aiming for explosion-free DED deposition. Before coating, all panels are thoroughly cleaned with acetone to remove oil and dirt and ensure even absorption of laser energy.

The KUKA robotic arm with six degrees of freedom is linked to a laser cladding head consisting of a powder feeder nozzle and laser. The laser uses the Laser line LDF 4.000–100 fiber-coupled diode laser featuring a 5.5 mm spot diameter and a power capacity of 4000 W. Powder is got through a UNIQUECOAT gravimetric powder feeder, aligned coaxially with the laser beam.

Table 2. Chemical compound of SS316 material

El	C	Cr	Mn	Mo	N	Ni	P	S	Si	Fe
W	0.08	18	2	3	0.10	14	0.045	0.03	0.75	62

Table 3. Chemical compound of stellite-6 coating material

El	Co	Cr	W	C	Fe	Ni	Mn	Si	Mo
W	65.48	28	5	1.4	0.03	0.03	0.02	0.02	0.02

Argon serves dual purposes: shielding the melt-pool from decay and acting as a runner gas for powder feeding. Throughout the experiment, both the Standoff Distance (SOD) and inert gas flow rate remain constant. For microstructure examination, deposited samples are sliced using wire EDM in a cross direction at two different positions. Subsequently, these samples undergo thorough polishing using various grades of sandpaper and velvet cloth by following standard procedure. The setup of the LCP is shown in Figure 3.

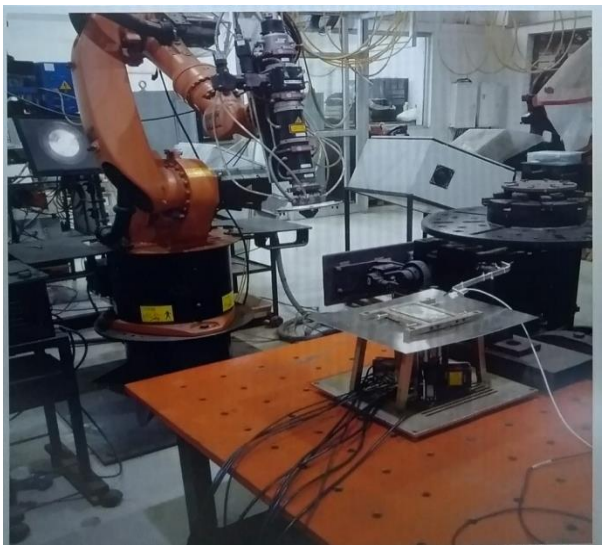

Fig. 3 Laser cladding process set up

Following the attainment of a mirror finish, a thorough examination was conducted utilizing both an optical microscope and SEM. The microstructure and elemental composition at critical locations were scrutinized using an EDS setup integrated with an SEM [JEOL 6380A]. The micro-hardness assessment was performed employing a Vickers hardness tester (Mitutoyo HM-200, Autovick) with a 200 g load and an 18-second dwell period. Detailed specifications of the LCP equipment are provided in Table 4.

To achieve a perfect surface, the SS316 specimen underwent deburring after initial cleaning procedures. Subsequently, the specimen was meticulously polished to eliminate scratches using polished sheets with varying particle sizes. Polish papers ranging from 200 to 1200 µm in particle dimensions were applied to the substrate. A lap wheel was used to further refine the sample surface to get a mirror quality on the testing surfaces.

Table 4. Specifications of the LC equipment

Laser	Fiber coupled diode laser
Make	Laser line
Capacity	4 KW (Max)
Laser Spot Diameter	5.5 mm
Standoff Distance	23 mm
Shielding Gas, Carrier Gas	Argon
Powder Feeder	UNICOATE Gravimetric Powder Feeder
Single Track Length	55 mm
Multi Track Length	55 mm (50% overlap)
Base Metal	SS316 (Melting point: -1375-1400 ^{o}c, Microhardness- 220-277 HV)
Cladding Material	Stellite-6 (Melting point: -1265-1354 ^{o}c, Microhardness-380-450 HV)

A track of Stellite-6 on SS316 is used to clad the single-layer samples. Figure 4 shows the result of the following parameters: LP 500 W, SS 20 mm/sand, PFR 30 g/min. It shows that the powder does not fuse at lower laser powers.

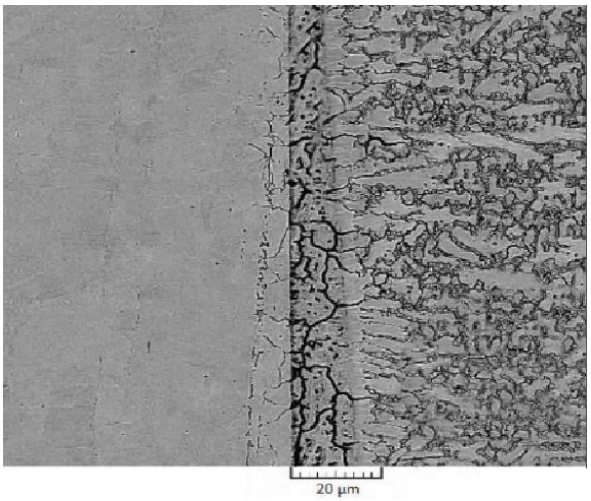

Fig. 4 No bonding between Stellite-6 and SS316

Figure 5 shows the result of the following parameters: LP 3800 W, SS 20 mm/s and PFR 30 g/min. It shows that the superfine powder fuses before being deposited on the material at high laser power.

Fig. 5 Overburning of stellite-6 and SS316

Multiple experiments were conducted involving the addition of Stellite-6 alloy powder to an SS316 substrate using LCP. Various combinations of LP, SS, and PFR of the LCP were assessed. Through the Taguchi L9 orthogonal array method, an optimal range of laser processing parameters was determined.

Three primary input parameters were considered: LP (W), SS (mm/s), and PFR (g/min). The range of different parameters is detailed in Table 5.

Table 5. Range of parameters

Sample No.	LP (W)	SS (mm/s)	PFR (g/min)
1	2600	15	40
2	2900	25	40
3	3200	20	40
4	2600	20	45
5	2900	15	45
6	3200	25	45
7	2600	25	50
8	2900	20	50
9	3200	15	50
Laser Spot Diameter	5.5 mm	Standoff Distance	23 mm
Shielding Gas	Argon	Carrier Gas	Argon

5. Characterization - Results and Discussion

A track of stellite-6 on SS316 is used to clad the single layer samples. At the lower LP 500 W, the powder does not fuse. At the value of higher LP 3800 W, the superfine powder fuses before being deposited on the material

Figures 6 depict the transverse sampling of the specimen; no surface fissure was seen on any of the specimens. All of the cladding specimens had no porousness and a strong articulate alliance with the base metal when the deposition was done under ideal process conditions.

Fig. 6 Experiment image

5.1. Optical Microscopy Test

The main components of a light microscope are the illumination system, objective lens, eyepiece, photomicrographic system, and specimen stage. The main tool used by researchers and technologists to investigate the microstructure of materials is light or optical microscopy. The

three main optical concepts of a microscope are resolution, magnification, and image creation. Only in as much as the characteristics resolved by the microscope are visible to the human eye can magnification have any significance. A meaningful magnification is high enough to make the microscopic details visible through a microscope. A good microscope should expand details to the human eye's resolution of roughly 0.2 mm. High magnification alone will not reveal a microscale item in a material specimen. Figure 7 to 15 show the optical images of specimen no 1 to 9. It shows the height and width of clad at different ranges of parameters.

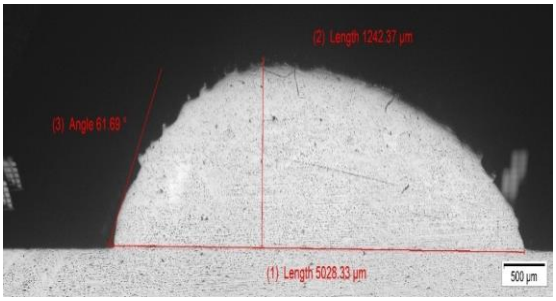

Fig. 7 Specimen no. 1

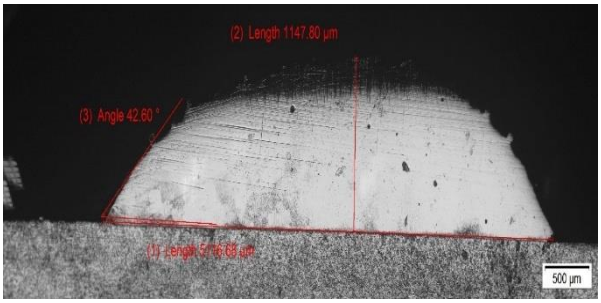

Fig. 8 Specimen no. 2

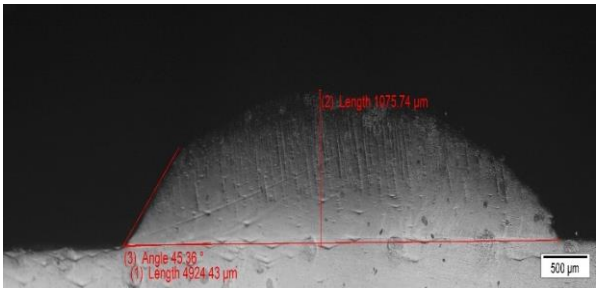

Fig. 9 Specimen no. 3

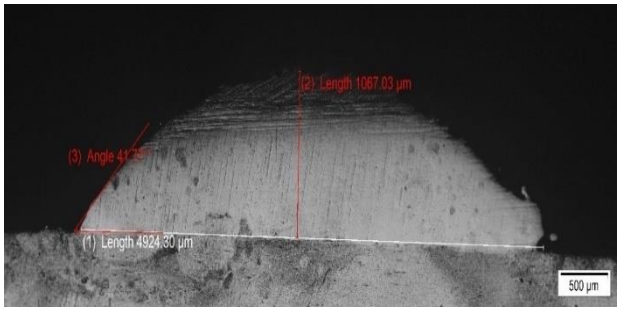

Fig. 10 Specimen no. 4

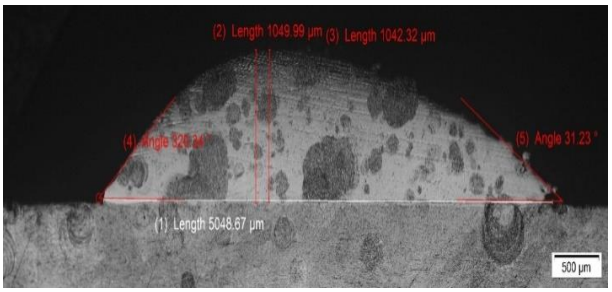

Fig. 11 Specimen no. 5

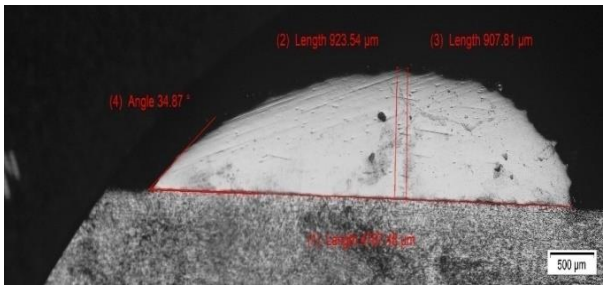

Fig. 12 Specimen no. 6

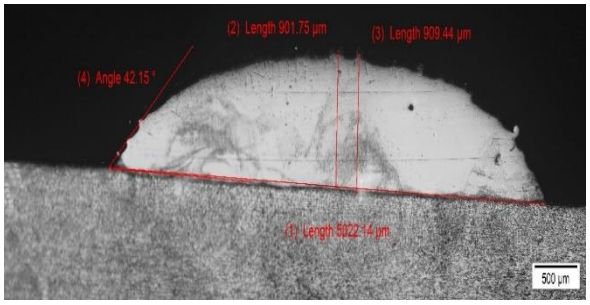

Fig. 13 Specimen no. 7

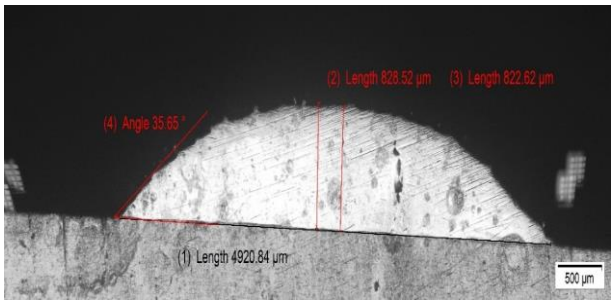

Fig. 14 Specimen no. 8

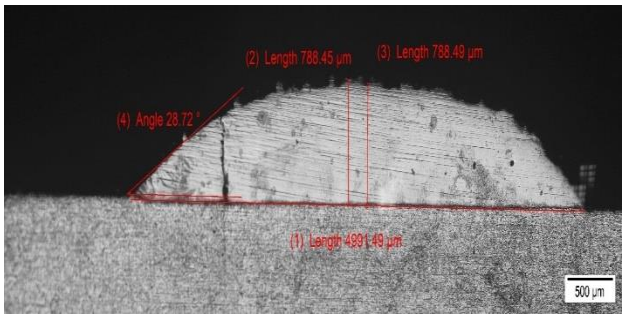

Fig. 15 Specimen no. 9

5.2. Clad Height

One of the most important computative elements of the clad structure is the CH. As the SS increases, the CH decreases, as seen in Figure 4. This phenomenon is caused by a decrease in contact time due to an increase in SS. As a result, the amount of molten cladding material that is deposited in the melt pool has less volume. The PFR is just as important in establishing the CH as the laser SS [43, 44]. Figure 6 illustrates how an increase in the PFR causes a rise in clothing height. On the other hand, raising the PFR causes the amount of powder per unit area to rise, which raises the CH [45]. Based on the previous discussion, it was determined that a maximum PFR of 50 g/min and a maximum SS of 25 mm/s may result in a maximum CH of 1242.37 mm.

5.3. Clad Width

As can be seen in Figure 5, with a fixed cladding PFR, the cladding width decreases linearly with an increase in laser SS, roughly matching the beam diameter. This linear relationship can be explained by the fact that, as SS increases, less LP is available per unit length, which results in less heat being available through the laser beam at the base material surface. The PFR negatively impacts CW. Because less LP was used to melt the coated material, the decrease in PFR resulted in a reduction in CW [43, 44]. from the single-clad structure's morphology in Figure 7. After conducting a parametric analysis and optimization study for the laser cladding of stellite-6 powder on SS316, we discovered that, at a laser SS of 25 mm/s and a PFR of 40 g/min, we can obtain the maximum width of 5116.68 mm.

Table 6. Experiment results

Sp. No.	LP (W)	SS (mm/s)	PFR (g/min)	CH (µm)	CW (µm)	Angle (°)
1	2600	15	40	1242.37	5028.33	61.69
2	2900	25	40	1147.80	5116.68	42.60
3	3200	20	40	1075.74	4924.43	45.36
4	2600	20	45	1067.03	4924.30	41.77
5	2900	15	45	1049.99	5048.67	31.23
6	3200	25	45	923.54	4787.48	34.87
7	2600	25	50	901.75	5022.14	42.15
8	2900	20	50	828.52	4920.84	35.65
9	3200	15	50	788.45	4991.49	28.72

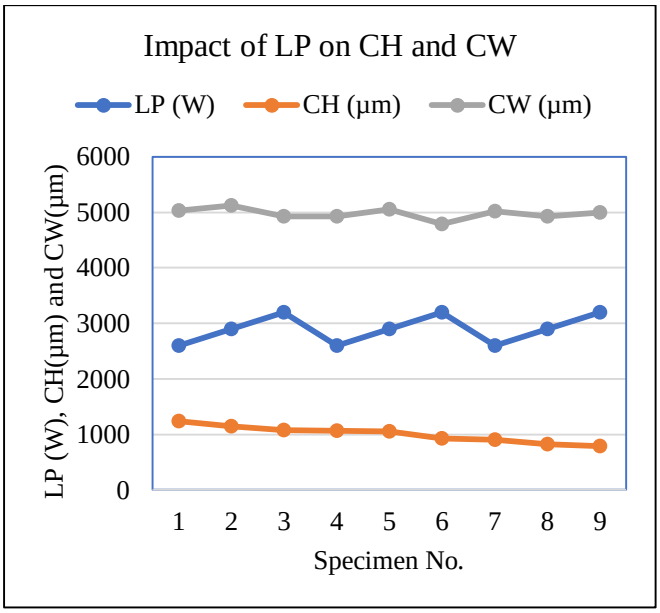

Fig. 16 Impact of LP on the CH and CW

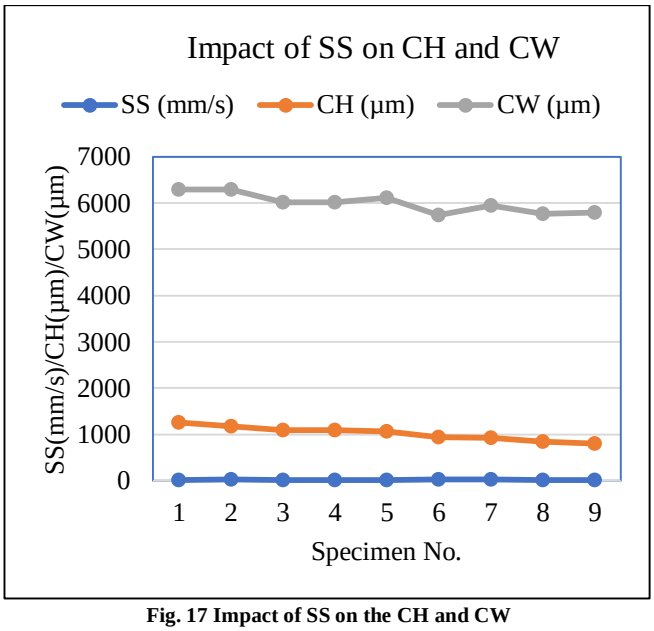

Fig. 17 Impact of SS on the CH and CW

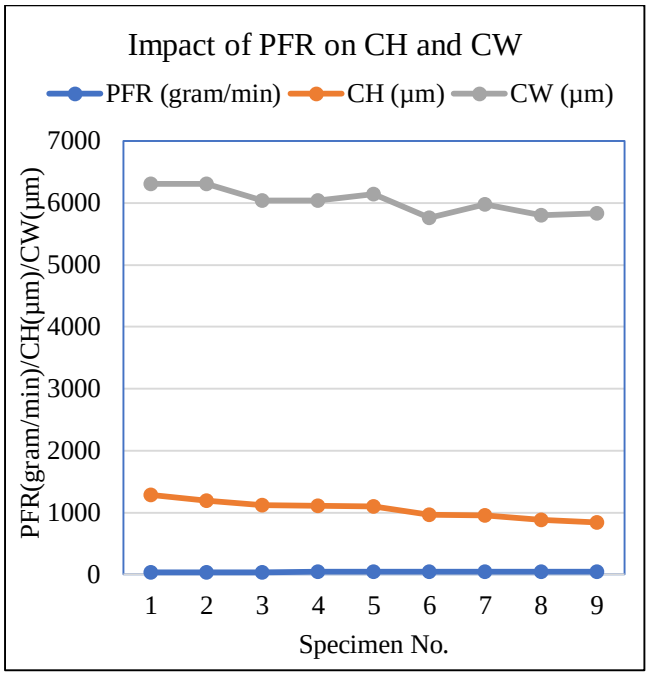

Fig. 18 Impact of the PFR on the CH and CW

Table 7. Impact of the parameters on the CH and CW

Parameters	CH	CW
LP	Decreases	I-Increases and E-Decreases
SS	Decreases	Increases
PFR	Decreases	Increases

Table 6 shows the clad height and clad width of specimen no. 1 to 9. With an increase in the LP, the CH decreases, but the CW initially increases but ultimately decreases. An increase in the SS, the CH decreases, but the CW increases. With an increase in the PFR, the CH decreases, but the CW increases.

5.4. SEM Analysis

Scanning electron microscopy is the most widely used type of electron microscope, providing morphological data and detail with unlimited depth at magnifications from 10x to 300,000x. It studies the microstructure by analyzing the surface of the material, similar to a confocal microscope, but with higher resolution and greater depth of field. SEM images are created by a focused beam of electrons that scans an area of a sample.

Table 8. Chemical composition of specimens 1 to 9

El (wt%)	Co	Cr	C	Ni	W	Fe	O	Mo
Sp. 1	51.27	28.30	7.45	5.69	4.47	1.05	0.97	0.81
Sp. 2	53.31	28.29	6.45	5.57	3.93	1.58	0.03	0.83
Sp. 3	52.20	28.45	6.85	5.66	3.99	1.39	0.86	0.60
Sp. 4	53.24	28.18	6.42	5.42	4.07	1.26	0.61	0.78
Sp. 5	52.49	27.98	6.14	5.61	4.38	1.64	0.82	0.94
Sp. 6	53.33	28.18	6.46	5.27	4.28	1.32	0.56	0.60
Sp. 7	53.20	28.52	6.01	5.58	4.31	1.18	0.62	0.48
Sp. 8	51.97	28.48	6.98	5.79	4.29	1.23	0.53	0.73
Sp. 9	52.29	28.19	7.01	5.38	4.22	1.23	0.76	0.92

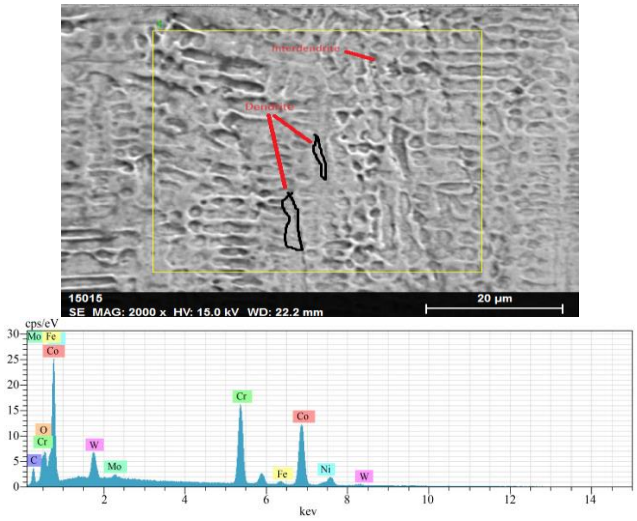

Fig. 19 EDS examination in the top region of one-layer coating

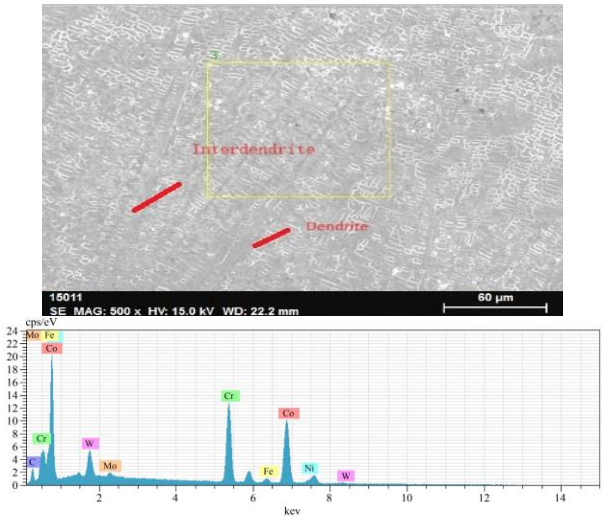

Fig. 20 EDS examination in the bottom region of the one-layer coating

Table 9. EDS results for top region

Region		Weight % of Elements							
		Co	Cr	C	Ni	W	Fe	O	Mo
Top	Dendritic	53.30	28.04	6.45	5.83	3.93	1.60	0.00	0.84
	Interdendritic	55.78	28.34	2.88	7.74	2.39	1.90	0.00	0.97

Table 10. EDS results for bottom region

Region		Weight % of Elements							
		Co	Cr	C	Ni	W	Fe	O	Mo
Bottom	Dendritic	51.29	28.28	7.46	5.68	4.47	1.06	0.96	0.81
	Interdendritic	53.10	29.48	3.59	6.87	4.88	0.79	0.31	0.98

In addition, EDS analysis was performed to examine segregation at various locations within the deposited layer. This study examines the dendritic and interdendritic zones at two locations within the deposit, namely, the top region and the bottom interface region, as depicted in Figures 19 and 20. Table 8 displays the tabulated EDS data for the one-layer sample. This indicates that the top portion of the layer has faster element segregation than the interface/lower section.

This situation can be described by directed curing, in which heat dissipates to the base metal, causing the bottom region to stiffen quickly and the clad top portion to stiffen toward the end. It becomes enhanced in Cr, Co and Ni by the time it solidifies, leading to strong segregation with 28.04% Cr, 53.30% Co, and 5.83% Ni in the dendritic zones and 28.34% Cr, 55.78% Co, and 7.74% Ni in the interdendritic zones. This component's strength and toughness are increased by the Cr, Co and Ni rich intermetallic phases [42].

5.5. MH Analysis

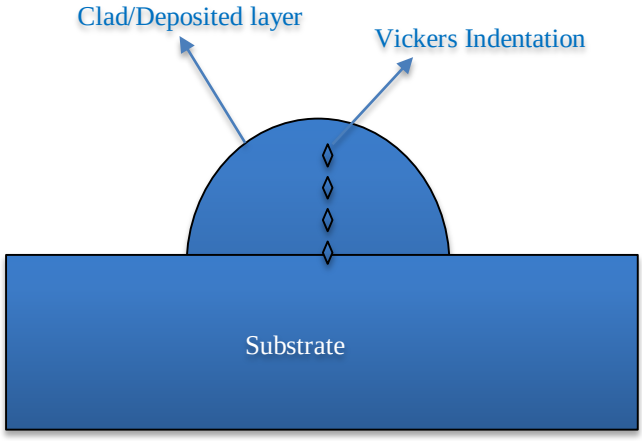

Fig. 21 Sketch of the MH measures along CH

This means that the hardness of the samples is greater than that of the coating material of Stellite-6 (Approximately 450 HV). In a one-layer sample, a maximum hardness of 469.3 HV is noted. When materials are repeatedly heated and cooled, elemental segregation decreases, increasing the hardness of the deposition. A resilient Ni matrix depleted of Co, Mo, and Cr is the result of this segregation; greater hardness values were observed as a result. Furthermore, studies were conducted to determine how the hardness varied with depth.

MH measures along the CH are shown in the schematic Figure 22, where the CH is measured at equivalent time intervals of 0.15 mm to 0.20 mm from the substrate to the clad contact. There was an abrupt rise in the hardness. For every test sample, there was an abrupt increase in the rigidity in the clad region compared to that at the interface. This might be the result of Fe diffusing into the clad zone from the base metal due to the infusion effect. EDS examination at the area of interface for a one-layer sample clearly demonstrated this diffusion; Table 8 indicates that a 53.30% Co concentration at the area of interface resulted in a high hardness.

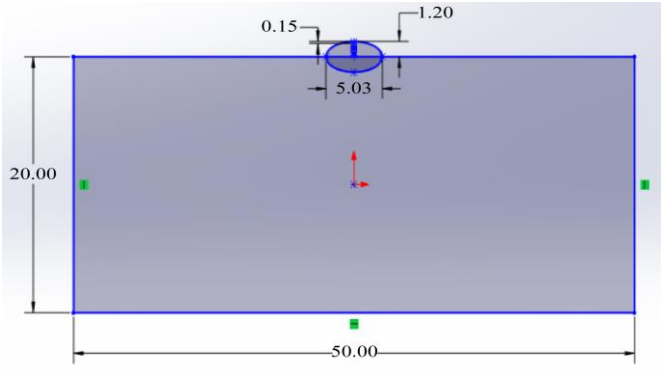

Fig. 22 Sketch of the MH measures along CH

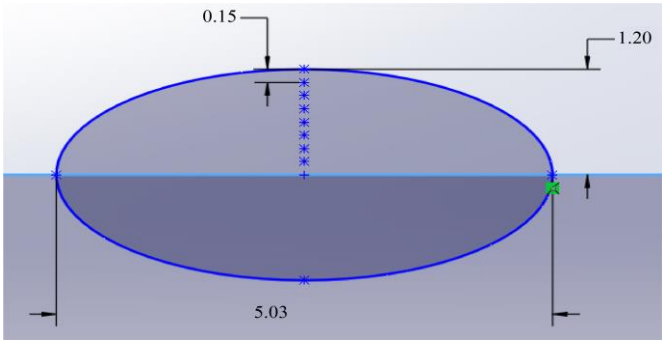

Fig. 23 Sketch of the MH measures along CH

This means that the hardness of the samples is greater than that of the coating material of Stellite-6 (Approximately 450 HV). In a one-layer sample, a maximum hardness of 469.3 HV is noted. When materials are repeatedly heated and cooled, elemental segregation decreases, increasing the hardness of the deposition. A resilient Ni matrix depleted of Co, Mo, and Cr is the result of this segregation; greater hardness values were observed as a result.

Furthermore, studies were conducted to determine how the hardness varied with depth. MH measures along the CH are shown in the schematic Figure 22, where the CH is measured at equivalent time intervals of 0.15 mm to 0.20 mm from the substrate to the clad contact. There was an abrupt rise in the hardness. For every test sample, there was an abrupt increase in the rigidity in the clad region compared to that at the interface. This might be the result of Fe diffusing into the clad zone from the base metal due to the infusion effect. EDS examination at the area of interface for a one-layer sample clearly demonstrated this diffusion; Table 8 indicates that a 53.30% Co concentration at the area of interface resulted in a high hardness.

Table 11. MH test results

POI/S.No.	Sp. No.1	Sp. No.2	Sp. No.3	Sp. No.4	Sp. No.5	Sp. No.6	Sp. No.7	Sp. No.8	Sp. No.9
POI-1	228.6	226.1	224.1	222.3	223.5	223.4	224.2	224.4	221.5
POI-2	367.1	347.2	341.2	347.2	351.1	349.1	356.1	361.1	348.1
POI-3	402.1	405.1	402.4	401.2	408.1	411.1	400.1	403.1	413.2
POI-4	423.1	421.7	414.2	417.3	419.3	426.8	417.8	418.6	429.1
POI-5	431.7	438.1	433.9	434.6	439.1	442.1	432.5	438.4	438.6
POI-6	442.1	447.1	448.1	441.2	444.4	449.1	445.8	449.1	447.2
POI-7	461.2	463.2	462.3	466.5	468.1	469.3	464.2	465.2	466.8

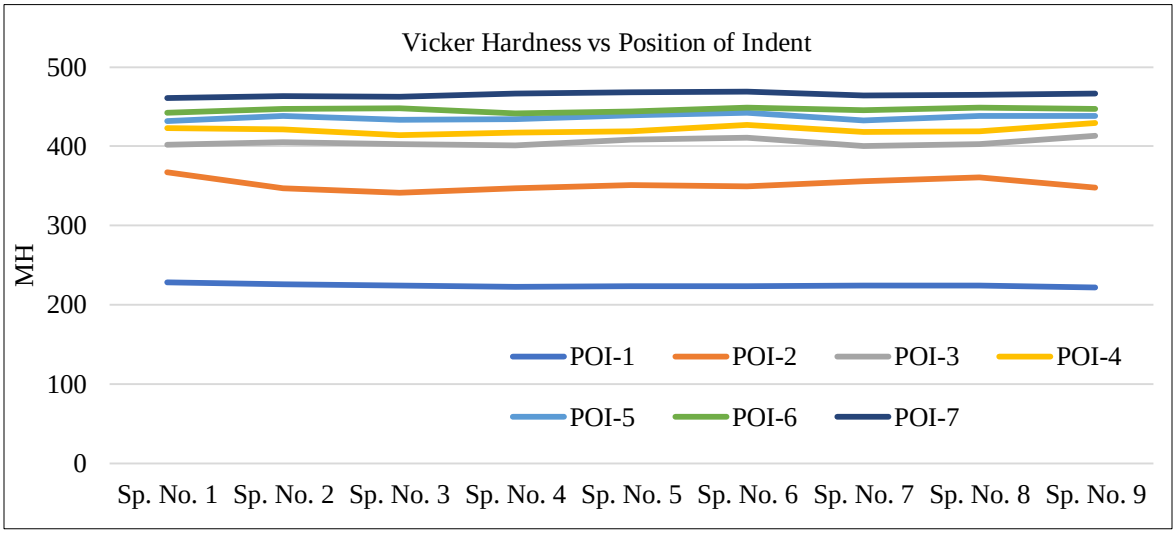

Fig. 24 Vickers hardness vs. Position of the indent

5.6. Dye Penetration Test

One of the earliest and most basic types of non-destructive inspection is the Dye Penetration Test (DPT). The Dye Penetrant Test also called the Liquid Penetrant Test, is a popular method for identifying surface irregularities such as fractures, fissures, porosity, grinding defects, partial fusion, and joint faults. Finding anomalies in materials such as Al, CI, Brass, Steel and SS, Cu, Mg, Carbides, Stellite, Ceramics, and some plastics is made easier with the help of this test or inspection technique. Accordingly, the dye penetration test is very cost-effective when compared to other non-destructive inspection techniques and appropriate for both ferrous and non-ferrous materials.

The capillary action theory underpins the Dye Penetration test. When a liquid is left on a clean, dry surface for a specific amount of time, known as the "Dwell Time," the liquid's low surface tension allows it to permeate. The test specimen or item must be covered with a liquid penetrating by dipping, spraying, or brushing. Once the dwell period has elapsed, the surplus must be removed. Sometimes, a developer is needed. The developer's primary job is to extract the penetrant from the defect and leave an invisible trail that the inspector can see. The dye penetration inspection is carried out in either white or ultraviolet light, depending on the type of dye utilized [46]. No surface defect was found on deposited specimens after DPT.

Fig. 25 Dye penetration test-1

Fig. 26 Dye penetration test-2

6. Conclusion

Single-layer stellite-6 deposition on the SS316 substrate was attempted utilizing the laser-aided DED procedure. The following conclusions were drawn after a careful examination of the optical microscopy, microstructure and hardness of the deposited samples:

With an increase in the LP, the CH decreases, but the CW initially increases but ultimately decreases.

With an increase in the SS, the CH decreases, but the CW increases.

With an increase in the PFR, the CH decreases, but the CW increases.

The cladding process increases the hardness of the cladding material more than the actual hardness of the substrate material, which tends to increase the wear resistance and corrosion resistance properties of the coating material.

For a one-layer sample, the maximum hardness is 469.3 HV, and the minimum is 221.5 HV. The exhaustion of fortification elements in the Cr, Co, and Ni forms due to decreasing segregation is the source of the increasing trend in hardness. The laser cladding process provides a good surface finish on deposited samples.

Acknowledgments

The authors would like to thank VNIT Nagpur for permitting us to conduct experiments in their laboratories. The authors also want to thank M/s Shreenath Engineering Industries, Nagpur, for letting us conduct practicals using their LC resource.

References

[1] T.H. Maiman, "Stimulated Optical Radiation in Ruby," *Nature*, vol. 187, no. 4736, pp. 493-494, 1960. [CrossRef] [Google Scholar] [Publisher Link]

[2] T.H. Maiman et al., "Stimulated Optical Emission in Fluorescent Solids. II. Spectroscopy and Stimulated Emission in Ruby," *Physical Review*, vol. 123, no. 4, pp. 1151-1157, 1961. [CrossRef] [Google Scholar] [Publisher Link]

[3] W.M. Steen, "Laser Material Processing-An Overview," *Journal of Optics A: Pure and Applied Optics*, vol. 5, no. 4, 2003. [CrossRef] [Google Scholar] [Publisher Link]

[4] Theodore H. Maiman, "Laser Applications," *Physics Today*, vol. 20, no. 7, pp. 24-28, 1967. [CrossRef] [Google Scholar] [Publisher Link]

[5] W.M. Steen, *Laser Material Processing*, Germany: Springer, pp. 1-408, 2003. [Google Scholar] [Publisher Link]

[6] Ehsan Toyserkani, Amir Khajepour, and Stephen F. Corbin, *Laser Cladding*, 1st ed., CRC Press, pp. 1-280, 2004. [CrossRef] [Google Scholar] [Publisher Link]

[7] K. Komvopoulos, and K. Nagarathnam, "Processing and Characterization of Laser-Cladded Coating Materials," *Journal of Engineering Materials and Technology*, vol. 112, no. 2, pp. 131-143, 1990. [CrossRef] [Google Scholar] [Publisher Link]

[8] L. Han, K.M. Phatak, and F.W. Liou, "Modeling of Laser Cladding with Powder Injection," *Metallurgical and Materials Transactions B*, vol. 35, pp. 1139-1150, 2004. [CrossRef] [Google Scholar] [Publisher Link]

[9] Liaoyuan Chen et al., "Repair of Spline Shaft by Laser-Cladding Coarse TiC Reinforced Ni-Based Coating: Process, Microstructure and Properties," *Ceramics International*, vol. 47, no. 21, pp. 30113-30128, 2021. [CrossRef] [Google Scholar] [Publisher Link]

[10] Minjie Song et al., "Effects of Laser Cladding on Crack Resistance Improvement for Aluminum Alloy Used in Aircraft Skin," *Optics & Laser Technology*, vol. 133, 2021. [CrossRef] [Google Scholar] [Publisher Link]

[11] Corbin M. Grohol, Yung C. Shin, and Alex Frank, "Laser Cladding of Aluminum Alloy 6061 via Off-Axis Powder Injection," *Surface and Coatings Technology*, vol. 145, 2021. [CrossRef] [Google Scholar] [Publisher Link]

[12] Ehsan Toyserkani, Amir Khajepour, and Stephen Corbin, "3-D Finite Element Modeling of Laser Cladding by Powder Injection: Effects of Laser Pulse Shaping on the Process," *Optics and Lasers in Engineering*, vol. 41, no. 6, pp. 849-867, 2004. [CrossRef] [Google Scholar] [Publisher Link]

[13] Kaiming Wang et al., "Microstructure and Properties of WC Reinforced Ni-Based Composite Coatings with Y2O3 Addition on Titanium Alloy by Laser Cladding," *Science and Technology of Welding and Joining*, vol. 24, no. 5, pp. 517-524, 2019. [CrossRef] [Google Scholar] [Publisher Link]

[14] Jin Ke et al., "Microstructure and Fretting Wear of Laser Cladding Self-Lubricating Anti-Wear Composite Coatings on TA2 Alloy after Aging Treatment," *Optics & Laser Technology*, vol. 119, 2019. [CrossRef] [Google Scholar] [Publisher Link]

[15] Shitanshu Shekhar Chakraborty, and Samik Dutta, "Estimation of Dilution in Laser Cladding Based on Energy Balance Approach Using Regression Analysis," *Sādhanā*, vol. 44, 2019. [CrossRef] [Google Scholar] [Publisher Link]

[16] Ondřej Nenadl et al., "The Prediction of Coating Geometry from Main Processing Parameters in Laser Cladding," *Physics Procedia*, vol. 56, pp. 220-227, 2014. [CrossRef] [Google Scholar] [Publisher Link]

[17] Kaiming Wang et al., "Microstructure and Property of Laser Clad Fe-Based Composite Layer Containing Nb and B4C Powders," *Journal of Alloys and Compounds*, vol. 802, pp. 373-384, 2019. [CrossRef] [Google Scholar] [Publisher Link]

[18] Fuquan Li et al., "Microstructural Study of MMC Layers Produced by Combining Wire and Coaxial WC Powder Feeding in Laser Direct Metal Deposition," *Optics & Laser Technology*, vol. 77, pp. 134-143, 2016. [CrossRef] [Google Scholar] [Publisher Link]

[19] Kaiming Wang et al., "A Study on the Additive Manufacturing of a High Chromium Nickel-Based Superalloy by Extreme High-Speed Laser Metal Deposition," *Optics & Laser Technology*, vol. 133, 2021. [CrossRef] [Google Scholar] [Publisher Link]

[20] Shrey Bhatnagar, Suvradip Mullick, and Muvvala Gopinath, "A Lumped Parametric Analytical Model for Predicting Molten Pool Temperature and Clad Geometry in Pre-Placed Powder Laser Cladding," *Optik*, vol. 247, 2021. [CrossRef] [Google Scholar] [Publisher Link]

[21] Waheed Ul Haq Syed, Andrew J. Pinkerton, and Lin Li, "A Comparative Study of Wire Feeding and Powder Feeding in Direct Diode Laser Deposition for Rapid Prototyping," *Applied Surface Science*, vol. 247, no. 1-4, pp. 268-276, 2005. [CrossRef] [Google Scholar] [Publisher Link]

[22] Adrita Dass, and Atieh Moridi, "State of the Art in Directed Energy Deposition: From Additive Manufacturing to Materials Design," *Coatings*, vol. 9, no. 7, pp. 1-26, 2019. [CrossRef] [Google Scholar] [Publisher Link]

[23] U. de Oliveira, V. Ocelík, and J.Th.M. De Hosson, "Analysis of Coaxial Laser Cladding Processing Conditions," *Surface and Coatings Technology*, vol. 197, no. 2-3, pp. 127-136, 2005. [CrossRef] [Google Scholar] [Publisher Link]

[24] Mingzhong Hao, and Yuwen Sun, "A FEM Model for Simulating Temperature Field in Coaxial Laser Cladding of TI6AL4V Alloy Using an Inverse Modeling Approach," *International Journal of Heat and Mass Transfer*, vol. 64, pp. 352-360, 2013. [CrossRef] [Google Scholar] [Publisher Link]

[25] Chun-Sheng OuYang et al., "Preparation and High Temperature Tribological Properties of Laser In-Situ Synthesized Self-Lubricating Composite Coating on 304 Stainless Steel," *Journal of Materials Research and Technology*, vol. 9, no. 4, pp. 7034-7046, 2020. [CrossRef] [Google Scholar] [Publisher Link]

[26] Xixi Luo et al., "Effect of Line Energy Density of the Laser Beam on the Microstructure and Wear Resistance Properties of the Obtained Fe3Al Laser Cladding Coatings," *Optik*, vol. 261, 2022. [CrossRef] [Google Scholar] [Publisher Link]

[27] Can Huang et al., "Dry Sliding Wear Behavior of Laser Clad TiVCrAlSi High Entropy Alloy Coatings on Ti–6Al–4V Substrate," *Materials & Design*, vol. 41, pp. 338-343, 2012. [CrossRef] [Google Scholar] [Publisher Link]

[28] T.E. Abioye, D.G. McCartney, and A.T. Clare, "Laser Cladding of Inconel 625 Wire for Corrosion Protection," *Journal of Materials Processing Technology*, vol. 217, pp. 232-240, 2015. [CrossRef] [Google Scholar] [Publisher Link]

[29] Gang Wang et al., "Tribological Study of Ti3SiC2/Cu5Si/TiC Reinforced Co-Based Coatings on SUS304 Steel by Laser Cladding," *Surface and Coatings Technology*, vol. 432, 2022. [CrossRef] [Google Scholar] [Publisher Link]

[30] Hussam El Cheikh et al., "Analysis and Prediction of Single Laser Tracks Geometrical Characteristics in Coaxial Laser Cladding Process," *Optics and Lasers in Engineering*, vol. 50, no. 3, pp. 413-422, 2012. [CrossRef] [Google Scholar] [Publisher Link]

[31] M.J. Hamedi, M.J. Torkamany, and J. Sabbaghzadeh, "Effect of Pulsed Laser Parameters on In-Situ TiC Synthesis in Laser Surface Treatment," *Optics and Lasers in Engineering*, vol. 49, no. 4, pp. 557-563, 2011. [CrossRef] [Google Scholar] [Publisher Link]

[32] André A. Ferreira et al., "Optimization of Direct Laser Deposition of a Martensitic Steel Powder (Metco 42C) on 42CrMo4 Steel," *Metals*, vol. 11, no. 4, pp. 1-18, 2021. [CrossRef] [Google Scholar] [Publisher Link]

[33] Bo Shan et al., "Laser Cladding of Fe-Based Corrosion and Wear-Resistant Alloy: Genetic Design, Microstructure, and Properties," *Surface and Coatings Technology*, vol. 433, 2022. [CrossRef] [Google Scholar] [Publisher Link]

[34] Zhengtao Gan et al., "Numerical Simulation of Thermal Behavior and Multicomponent Mass Transfer in Direct Laser Deposition of Co-Base Alloy on Steel," *International Journal of Heat and Mass Transfer*, vol. 104, pp. 28-38, 2017. [CrossRef] [Google Scholar] [Publisher Link]

[35] Damian Janicki, "Laser Cladding of Inconel 625-Based Composite Coatings Reinforced by Porous Chromium Carbide Particles," *Optics & Laser Technology*, vol. 94, pp. 6-14, 2017. [CrossRef] [Google Scholar] [Publisher Link]

[36] Fuxing Fu et al., "Analysis on the Physical Mechanism of Laser Cladding Crack and its Influence Factors," *Optik*, vol. 127, no. 1, pp. 200-202, 2016. [CrossRef] [Google Scholar] [Publisher Link]

[37] Prabu Balu et al., "Multi-Response Optimization of Laser-Based Powder Deposition of Multi-track Single Layer Hastelloy C-276," *Materials and Manufacturing Processes*, vol. 28, no. 2, pp. 173-182, 2013. [CrossRef] [Google Scholar] [Publisher Link]

[38] B. Cárcel et al., "Laser Cladding of TiAl Intermetallic Alloy on Ti6Al4V -Process Optimization and Properties," *Physics Procedia*, vol. 56, pp. 284-293, 2014. [CrossRef] [Google Scholar] [Publisher Link]

[39] Zhenguo Nie et al., "Experimental Study and Modeling of H13 Steel Deposition Using Laser Hot-Wire Additive Manufacturing," *Journal of Materials Processing Technology*, vol. 235, pp. 171-186, 2016. [CrossRef] [Google Scholar] [Publisher Link]

[40] C.J. Todaro et al., "Grain Structure Control During Metal 3D Printing by High-Intensity Ultrasound," *Nature Communications*, vol. 11, no. 1, pp. 1-9, 2020. [CrossRef] [Google Scholar] [Publisher Link]

[41] Guangyi Ma et al., "Microstructure Evolution and Mechanical Properties of Ultrasonic Assisted Laser Clad Yttria Stabilized Zirconia Coating," *Ceramics International*, vol. 43, no. 13, pp. 9622-9629, 2017. [CrossRef] [Google Scholar] [Publisher Link]

[42] Victor Geanta et al., "Chemical Composition Influence on Microhardness, Microstructure and Phase Morphology of AlxCrFeCoNi High Entropy Alloys," *Revista de Chimie*, vol. 69, no. 4, pp. 798-801, 2018. [CrossRef] [Google Scholar] [Publisher Link]

[43] S. Zhang, C.L. Wu, and C.H. Zhang, "Phase Evolution Characteristics of FeCoCrAlCuVxNi High Entropy Alloy Coatings by Laser High-Entropy Alloying," *Materials Letters*, vol. 141, pp. 7-9, 2015. [CrossRef] [Google Scholar] [Publisher Link]

[44] Prakash Kattire et al., "Experimental Characterization of Laser Cladding of CPM 9V on H13 Tool Steel for Die Repair Applications," *Journal of Manufacturing Processes*, vol. 20, no. 3, pp. 492-499, 2015. [CrossRef] [Google Scholar] [Publisher Link]

[45] H. Zhang et al., "Laser Cladding of Colmonoy 6 Powder on AISI316L Austenitic Stainless Steel," *Nuclear Engineering and Design*, vol. 240, no. 10, pp. 2691-2696, 2010. [CrossRef] [Google Scholar] [Publisher Link]

[46] P. Prokhorenko, N. Migun, and N. Dezhkunov, "Development of Penetrant Test Theory Based on New Physical Effects," *Non-Destructive Testing '92*, pp. 538-542, 1992. [CrossRef] [Google Scholar] [Publisher Link]